Journal of Power Sources 240 (2013) 503–509

Contents lists available at SciVerse ScienceDirect

Journal of Power Sources

journal homepage: www.elsevier.com/locate/jpowsour

Short communication

# Enhancing the performance of free-standing $TiO_2$ nanotube arrays based dye-sensitized solar cells via ultraprecise control of the nanotube wall thickness

Xianfeng Gao, Junhong Chen, Chris Yuan*

*Department of Mechanical Engineering, University of Wisconsin Milwaukee, Wisconsin 53211, USA*

## HIGHLIGHTS

- Fabricated free standing $TiO_2$ nanotube array with wall thickness between 10 and 30 nm.
- Investigated the dependence of DSC performance on nanotube wall thickness.
- Identified an optimal $TiO_2$ nanotube wall thickness at 450 ALD cycles for DSC.
- The best efficiency 4.65% obtained at 450 cycles is 1.8 times of that at 250 cycles.

## ARTICLE INFO

*Article history:*
Received 11 January 2013
Received in revised form
5 April 2013
Accepted 6 April 2013
Available online 25 April 2013

*Keywords:*
Solar cell
Titanium dioxide
Nanotube
Wall thickness

## ABSTRACT

Free standing $TiO_2$ nanotube (TNT) array film was fabricated via template-assisted Atomic Layer Deposition (ALD) in nanoporous anodic alumina templates followed by alumina dissolution. Effect of $TiO_2$ nanotube wall thickness on the photovoltaic performance was studied on the dye sensitized solar cells with the TNT wall thickness precisely controlled by ALD between 250 and 550 cycles. The results show that the photovoltaic performance can be improved by optimizing the TNT wall thickness. A thick enough tube wall is crucial for forming space charge layer to allow efficient charge separation, but too thick wall thickness will reduce dye loading relatively. A photovoltaic energy conversion efficiency of 4.65% was obtained on the device with 450 ALD cycles of TNT wall thickness, which is about 1.8 times of that obtained with 250 cycles thickness.

© 2013 Elsevier B.V. All rights reserved.

## 1. Introduction

Dye-sensitized solar cells (DSC) have attracted substantial interests in the past decades due to its low cost and high throughput manufacturing potential for large scale industrial applications [1–3]. Conventional DSCs are fabricated with mesoporous nanocrystalline $TiO_2$ photoelectrodes which have large internal surface areas for absorbing light-sensitive dyes. Upon illumination, electrons will be excited from the light-sensitive dyes and then injected into the wide bandgap $TiO_2$ nanostructured materials. However, conventional DSCs rely on a trap-limited diffusion mechanism for electron transport and collection in the mesoporous $TiO_2$ nanostructured materials [4]. The process is slow and inefficient which limit the photo conversion efficiency of the solar cells.

Highly ordered $TiO_2$ nanotube (TNT) electrodes have been demonstrated with better photovoltaic performance due to increased charge collection efficiency and enhanced light trapping ability [5,6]. Another major advantage of such one-dimensional nanostructure over planar geometries is that they can decouple the directions of light absorption and charge carrier collection [7–9]. However, the physical parameters of the $TiO_2$ nanotube arrays can be an obstacle because both the electric and photo property would be affected by the morphology [10–13]. It is especially important to control the physical parameters for optimizing the device performance of solar cells. Past research has successfully demonstrated the strong dependence of solar cell efficiency on nanotube length, in general with increased power efficiency on longer nanotubes [14,15]. It was estimated the electron diffusion length in TNT is of the order of 100 μm on titanium foil by considering the electron diffusion coefficient and lifetime as a function of electron quasi Fermi level [15], which indicate that electron collection in TNT arrays with varied tube lengths are all efficient and the improvement should contribute to dye loading and light absorption enhancement from the increased length. Therefore, it's reasonable to estimate that the main electrical

* Corresponding author. Tel.: +1 414 229 5639; fax: +1 414 229 6958.
*E-mail address:* cyuan@uwm.edu (C. Yuan).

0378-7753/$ – see front matter © 2013 Elsevier B.V. All rights reserved.
http://dx.doi.org/10.1016/j.jpowsour.2013.04.037

obstacle may originate from the electron injection process through the interface of dye and $TiO_2$, which are strongly affected by the TNT wall thickness [16,17]. However, it was rarely investigated experimentally before because of the challenges in ultraprecise control of the TNT wall thickness in nanometer scale.

In order to obtain nanotubes which are particularly favorable to achieve efficient charge injections with reduced charge recombination, ultraprecise control of the wall thickness of $TiO_2$ nanotubes will be highly desirable. To date, highly ordered TNT arrays are generally synthesized through two approaches: 1). Self-assembled method such as Ti electrochemical anodization [18–20], hydrothermal growth [21], etc., and 2). Template-assisted approaches usually through nanoporous anodic alumina oxide (AAO) template [22,23]. Although self-assembled method provide a more direct route to the arrays, but template assisted approach could provide more precise control of the tube dimensions especially combined with Atomic Layer Deposition (ALD) [24–26]. ALD is a self-limiting nanotechnology which operates in a cyclic process and can fabricate uniform and conformal layers at atomic scale [27–29], which satisfy the requirement of ultraprecise wall thickness control for the nanotube geometric study. Past research has applied ALD on a large number of metal oxides (such as ZnO, $TiO_2$, $ZrO_2$, $SnO_2$ and NiO) for new electrode development [28,30].

In this paper, we use free standing $TiO_2$ nanotube arrays as a model material for DSC fabrication and conduct a quantitative study on the effect of the TNT wall thickness on the solar device performance. The TNT wall thickness is controlled by various ALD deposition cycles in the range of 10–30 nm. From these results, we demonstrate that the efficiency of $TiO_2$ nanotube array based DSC can be improved by optimizing the wall thickness. An energy conversion efficiency of 4.65% was obtained using the TNT with 450 cycles $TiO_2$ deposition, which is about 1.8 times of that obtained using the TNT with 250 cycles. This geometric study of $TiO_2$ nanotube arrays can offer a strategy toward optimizing the energy conversion efficiency with other semiconductor materials in solar cell fabrication.

## 2. Experimental

### 2.1. Free-standing $TiO_2$ nanotube membrane fabrication

The $TiO_2$ nanotube was fabricated through a template ALD technique. Commercial AAO membranes with 200 nm pores (Anodisc, Whatman) were used as the template. Briefly, the AAO template was attached on a Si substrate with the open end facing up. Diffusion mode of a Cambridge Nanotech S100 ALD system was used to deposit $TiO_2$ into high aspect ratio AAO nano pores. HTDMA and

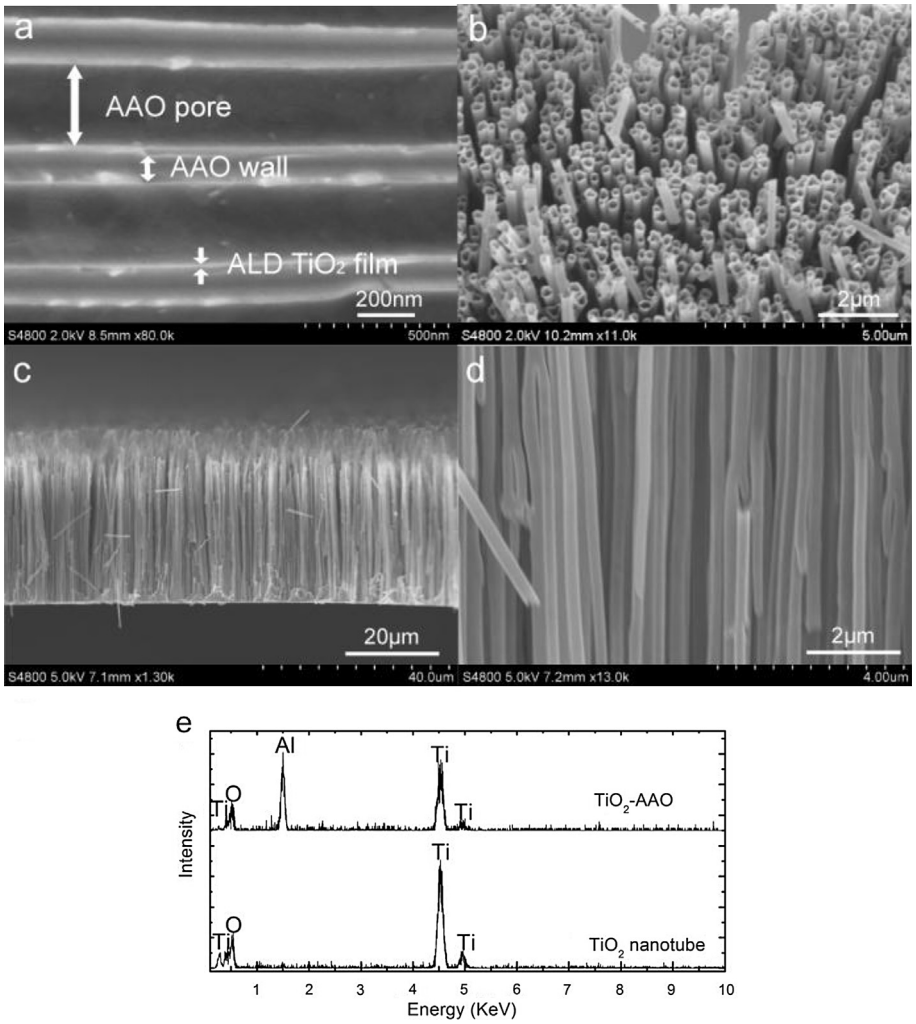


**Fig. 1.** (a) Cross section image of $TiO_2$ film deposited into AAO pores (b) top view of the obtained $TiO_2$ nanotube arrays after AAO etching. (c) Low magnification and (d) high magnification cross section image of $TiO_2$ nanotube array film. (e) EDS spectrum of $TiO_2$ nanotube before and after etching AAO.

water was introduced subsequently at a temperature of 200 °C using 8 s diffuse time and 8 s purging time between the two exposures. The wall thickness of $TiO_2$ nanotube was controlled by the deposition cycles. After deposition, the AAO/$TiO_2$ membrane was annealed at 450 °C in oxygen ambience for 2 h. To release free standing TNT array film, the annealed membrane was immersed into 1 M NaOH solution for 1 h. After the etching process, the sample was washed in DI water and then transferred into 100% hexamethyldisilazane (HMDS). 100% ethanol was used as a medium first to remove the water on the surface of the TNT film first since HMDS is not soluble with water. The TNT film was immersed into a graded series of water–ethanol mixtures gradually, which has the volume ratio of 2:1, 1:1, 1:2, and finally 100% ethanol. Once the sample was in 100% ethanol, it was transferred to 100% HMDS with the same procedure using a series of ethanol-HMDS mixture. Finally, the released TNT array film was dried in air at room temperature.

### 2.2. DSC fabrication

Free standing TNT array film was transferred to a fluorine-doped tin oxide (FTO) substrate which was covered by a thin layer $TiO_2$ paste (Solaronix, Ti-Nanoxide HT) formed by doctor blading. After being dried in air, the electrode was sintered at 450 °C for 30 min and subsequently cooled to 80 °C. The warm membrane was sensitized overnight in 0.5 mM $(Bu_4N)_2$–[Ru(4,4′-(COOH)-2,2′-bipyridine)$_2$(NCS)$_2$ ] (N719) in ethanol solution. A 50 μm thick Surlyn frame was sandwiched between the open-pore side of the membrane and a platinized FTO. The electrolyte, 50 mM iodide/triiodide in methoxypropionitrile, was injected from the side of the electrodes.

### 2.3. Characterization methods

A Hitachi S-4800 Scanning Electron Microscopy (SEM) and a Hitachi H9000NAR high resolution transmission electron microscopy (HRTEM) were used to characterize the morphology of the nanotubes. The TNT was dispersed in ethanol and onto a TEM grid. The composition of the obtained material was examined by Energy-dispersive X-ray spectroscopy (EDS), and the crystal structure of the obtained $TiO_2$ nanotube was further analyzed by X-ray diffraction spectrum (XRD). The *J–V* properties of $TiO_2$ nanotube based DSC were tested using a Keithley 2420 source meter under illumination of 100 mW $cm^{-2}$ provided by an oriel solar simulator. Dye loading was measured with Ocean Optics UV–VIS Spectrometer (SD2000 fiber optics) by testing the absorbance of N719 dyes desorbed from the electrode by 10 mM NaOH. Incident photon to charge carrier efficiency (IPCE) measurement was performed using Newport measurement kit with a 300 W Xe lamp source. The wavelength of light was tuned with a Newport CS260 monochromator.

## 3. Result and discussion

### 3.1. Free standing TNT arrays fabrication with ultraprecise control of wall thickness

To study the effect of TNT wall thickness on the photovoltaic performance, high aspect ratio free-standing TNT array films with ultraprecise controlled wall thickness were fabricated. The wall thicknesses of the obtained TNT are in the range of 10–30 nm as controlled through ALD deposition cycles between 250 and 550

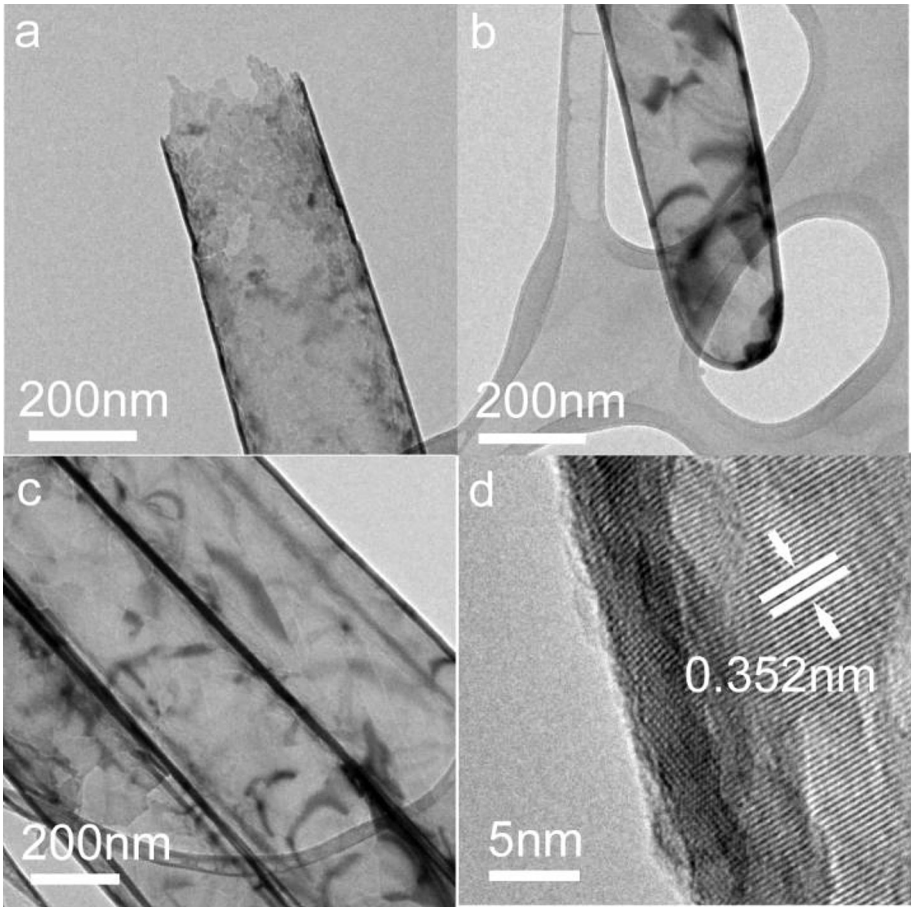


**Fig. 2.** TEM images of obtained $TiO_2$ nanotube. (a) Top and (b) bottom of $TiO_2$ nanotube (c) aligned $TiO_2$ nanotubes (d) HRTEM of the $TiO_2$ nanotube walls.

cycles. To obtain free-standing TNT arrays, a coaxial $TiO_2$/AAO nanostructure was first fabricated by atomic layer deposition of $TiO_2$ into the AAO template. For efficient high aspect ratio deposition, ALD was operated with the diffusion mode to allow sufficient surface reactions of precursors inside the deep trench of the AAO pores. Fig. 1 shows the cross-sectional image of AAO pore channels after $TiO_2$ deposition. As expected, the deposited $TiO_2$ films on the internal surface of the AAO are continuous and conformal. The AAO/$TiO_2$ film was put into 1 M NaOH solution for 1 h to etch away the AAO template after annealing at 450 °C in $O_2$ atmosphere. The sample was then washed carefully with DI water for several times. To obtain dry samples of the highly ordered free-standing TNT array film, hexamethyldisilazane (HMDS) evaporation method was used to avoid the bundling of the TNT arrays during the drying process which otherwise could lead to cracking of these TNT arrays [31–33]. Fig. 1b is the top view image of the obtained $TiO_2$ nanotube arrays released from the AAO template. Compact nanotube structure with open top end was formed and no destructive changes were observed after the release from the AAO template. In addition, cross-sectional images of the TNT arrays after the AAO removal are shown in Fig. 1c and d, respectively, with low and high magnifications. As shown in Fig. 1, the fabricated TNT arrays are in a highly ordered structure. The diameter of the nanotube is about 200 nm and the length is about 40 μm. Fig. 1e is the EDS spectrum of the AAO/$TiO_2$ sample before and after AAO etching. The Al peak and Ti peak resulting from AAO and $TiO_2$ respectively are shown on the upper level of the spectrum, indicating a successful $TiO_2$ deposition. The small carbon peak is from the carbon tape used to attach the film on the SEM stage. After etching away the AAO template (bottom in Fig. 1e), the Al peak disappears, indicating that the separation is thorough and complete. Moreover, no other elements are found in the EDS spectrum, suggesting there are no impurities and residues ever generated in the cleaning and evaporative drying process.

To characterize the detailed structure of a single $TiO_2$ nanotube, HRTEM was performed after dispersing $TiO_2$ nanotubes on a carbon-coated copper grid. Fig. 2a and b are HRTEM images of the top end and bottom end of a single $TiO_2$ nanotube with 350 cycles ALD deposition. The bottom image provides evidence that intact tube structure was formed and the diffusion mode of ALD was effective in supplying the precursors to the bottom of the AAO template. Fig. 2c shows the structure of aligned tubes. The wall thickness is about 18 nm as measured from HRTEM, indicating a deposition rate of 0.5 Å per ALD cycle, which is consistent with previously reported results [27]. Fig. 2d is the HRTEM image of the $TiO_2$ nanotube walls, which indicates a well prepared crystalline structure for the annealed nanotube. Lattice fringes in 0.352 nm are observed in the HRTEM image of the TNTs, corresponding to the (101) plane of anatase (JCPDS file no. 21-1272).

The crystalline structure of the TNT membrane was also confirmed with X-ray diffraction (XRD) patterns (Fig. 3). The deposited TNTs are amorphous and no peaks are found. In contrast, the diffraction peaks referred to anatase (JCPDS file no. 21-1272) of annealed $TiO_2$ are clearly observed after annealing, which is in agreement with the HRTEM result. All these characterized results confirm that the free-standing membrane fabricated in this process is only composed of $TiO_2$, no other impurities.

### 3.2. Effect of TNT wall thickness on DSC performance

The obtained free-standing TNT films were then transferred to an FTO substrate to fabricate front illumination DSCs for investigating the effect of the TNT wall thickness on DSC photovoltaic performance. Fig. 4 shows the current–voltage curves of DSCs based on various wall thicknesses of TNT films under AM1.5

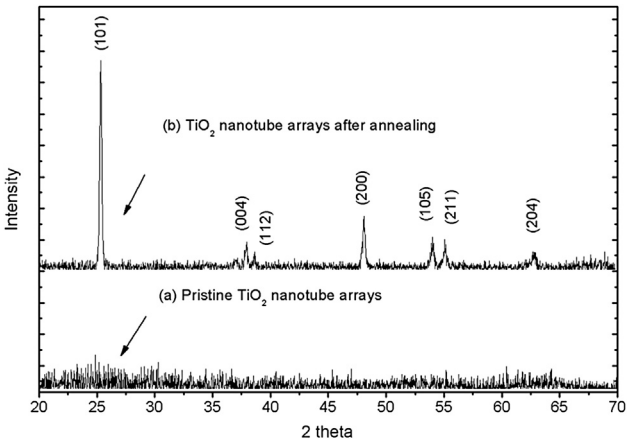


**Fig. 3.** XRD pattern of $TiO_2$ nanotube array film (a) before and (b) after annealing.

illumination. The inset shows the final structure of the fabricated solar cells. Detailed photovoltaic performance parameters of DSCs with different wall thickness TNT arrays are summarized in Table 1. Generally, all the devices fabricated in our experiments have high fill factors (>0.7), which indicate these devices are prepared well with small series resistance, good charge collection efficiency, and excellent contact between the free-standing TNTs and the FTO substrates. The DSC performance characterization also demonstrates the correlations between the photovoltaic performance and wall thickness clearly. The open circuit voltage ($V_{OC}$) and short circuit photocurrent densities ($J_{SC}$) increased with the wall thickness and reach a maximum value for 450 ALD cycles. Increasing the wall thickness to 550 ALD cycles did not improve them further. A highest photon-to-electricity conversion efficiency of 4.65% is obtained with TNTs of 450 ALD cycles, which is 80% higher than that obtained on 250 cycle ALD samples. Such a performance enhancement can be explained with the following mechanisms:

First, a critical wall thickness value is needed to obtain the best photo excited charge separation of the DSC. Considering the interface reaction when the semiconductor is immersed into the electrolyte, a space charge layer is generally developed in the semiconductor upon contact and equilibration with the electrolyte [34]. In the case of $TiO_2$-based solar cells, its initial Fermi level is

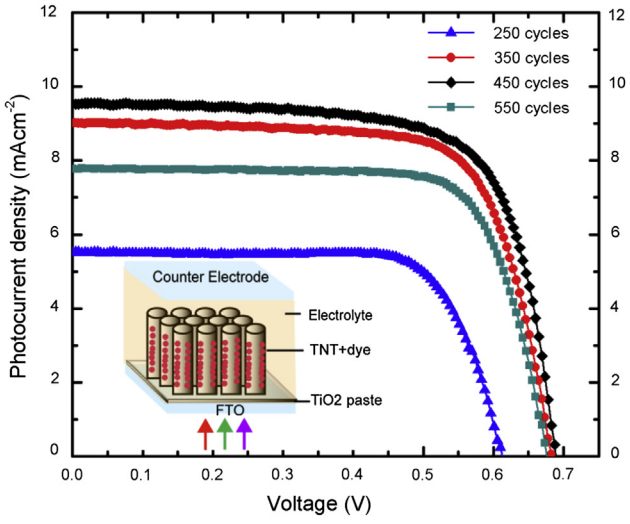


**Fig. 4.** *J–V* curves of fabricated solar cells based on varied wall thickness TNT.

**Table 1**
Photocurrent–voltage characteristics of the DSCs fabricated with TNTs under AM1.5 irradiation.

| ALD | $V_{OC}$ [V] | $J_{SC}$ [mA cm$^{-2}$] | FF | $\eta$ [%] |
|---|---|---|---|---|
| 250 cycles | 0.612 | 5.52 | 0.744 | 2.51 |
| 350 cycles | 0.682 | 9.01 | 0.718 | 4.41 |
| 450 cycles | 0.688 | 9.51 | 0.711 | 4.65 |
| 550 cycles | 0.676 | 7.79 | 0.745 | 3.92 |

$V_{OC}$, $J_{SC}$, ff and $\eta$ represent open circuit voltage, short circuit current, fill factor and power conversion efficiency, respectively.

above that of electrolyte, and accordingly the equilibration will be established by transferring electrons from $TiO_2$ to electrolyte, which will produce a depletion layer and the conduction band edge of $TiO_2$ would be bent upward, so as to establish a potential barrier against the injected electrons transferring back into the redox couples in the electrolyte [34,35]. The width of the depletion layer in $TiO_2$ can be calculated by [34]

$$\omega = \sqrt{\frac{2\varepsilon\varepsilon_0 V_B}{qN}} \quad (1)$$

where, $\varepsilon$ is the dielectric constant of $TiO_2$; $\varepsilon_0$ is the permittivity of free space; $q$ is the electronic charge; $N$ is the charge carrier concentration in $TiO_2$ and $V_B$ is the amount of band bending in the depletion layer, which has to be at least 50 mV in order to help the light-induced charge separation efficiently [17]. To utilize the upward band bending to prevent charge recombination, the sidewall thickness should reach a critical value to support the depletion layer. Otherwise, the thin wall may be depleted completely from the charge layer. In that case, the band bending could be negligibly small or even does not occur in the semiconductor [17]. For $TiO_2$ with anatase structure, the width of the depletion layer is about 12 nm as estimated from Equation (1) using $V_B = 50$ mV [36], $\varepsilon = 31$, [36] and $N = 10^{18}$ cm$^{-3}$ [36,37]. Considering the structure of the fabricated TNT arrays, the TNT wall thickness has to reach twice the depletion width (i.e., 24 nm) in order to support the depletion layer in the inner and the outer surfaces.

For the 250 cycle TNT arrays, the wall thickness is only about 12.5 nm which is much smaller than the critical thickness, and hence too thin to support the depletion layer (Fig. 5a). As a result, the thin wall was depleted completely and the band bending is negligible small. In this DSC device, the charge transport follows the same diffusion process as the traditional nanoparticle-based DSCs. In that mode, photogenerated electrons repeatedly interact with a distribution trap, which will undertake a random walk through the film [38]. Accordingly, the process is slow and can only collect a relatively small amount of charges in the electrode, which reduces the devices performance significantly. Similar phenomenon is observed from the work of Zhu et al., which showed that the electron transport time in about 8 nm wall thickness nanotubes is comparable with that in the nanoparticle film [5]. Because the wall thickness of the nanotube is too thin to support the depletion layer, the electron transport in it is dominated by the same diffusion process as in nanoparticle samples, resulting in a comparable transport time [5]. With the wall thickness increasing to the critical value to provide sufficient support for the depletion layer, potential barriers are then created near both the inner and the outer surfaces of the TNT nanotube (Fig. 5b), which leads to a decreased recombination of the collected electrons with the electrolyte. Consequently, the photo excited electrons will transport follow the rapid channel along the nanotube wall and sufficient amount of charges can be collected by the electrode. As a result, the $J_{SC}$ of the DSCs increases significantly with the increasing of the TNT wall thickness from 250 to 450 ALD cycles. Besides, the $J$–$V$ curves also show that the $V_{OC}$ of devices with thick walls (350, 450 and 550 ALD cycles) are much higher than that of the 250 cycles sample, which can also be attributed to the reduced recombination of electrons with the electrolyte on the $TiO_2$ tube surface. The experimental results are in good agreement with the theoretical modeling results presented by Ferber et al. [39]. Finally, it is worth noting that the difference of $J_{SC}$ between the samples of 350 cycles and 450 cycles is small, which means the electron transport enhancement induced by wall thickness increase is not significant when it is approaching the critical wall thickness. Once the wall thickness has reached the critical value to support the entire depletion layer, increasing the wall thickness further will neither increase the band bending nor provide extra benefit to reduce recombination, which will not help improve the photocurrent further. From the experimental results, it's reasonable to predict that the critical wall thickness to support band bending for efficient electron transport is around 23 nm

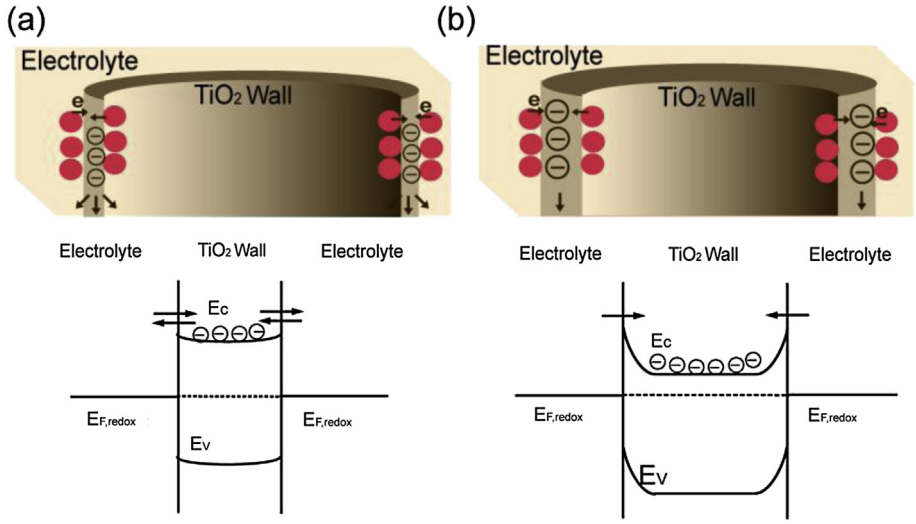


**Fig. 5.** Schematic diagram of nanotube based solar cell structure (a) and electron transportation and space charge layer formation in TNT with thick (b) and thin (c) wall in equilibrium with an electrolyte. $E_C$, $E_V$ and $E_F$ represent the conductive band, valence band and Fermi level of $TiO_2$ respectively. $E_{F,redox}$ represents the Fermi level of redox system in the electrode.

(corresponding with 450 cycles sample), which is consistent with the calculated result from Equation (1).

Secondly, increasing the TNT wall thickness will decrease the surface area of the electrodes and consequently lead to reduced dye absorption. The internal surface area can be characterized by roughness factor, defined as the total film area per unit substrate area. Approximately, the TNT has the same hexagonally arranged pores with AAO, and hence the roughness factors can be estimated by

$$\mathrm{RF} = \frac{4\pi rl}{\sqrt{3}d^2} \tag{2}$$

where $r$, $l$ and $d$ are the pore radius, pore length, and center-to-center pore spacing, respectively. From Equation (2), decreasing the pore radius will result in a lower RF. RF values can be calculated with an average original pore radius of 200 nm, pore spacing of 336 nm, and length of 40 μm as characterized from the SEM image. As calculated, the TNT nanotubes with wall thickness from 12.5 nm to 27.5 nm have RF values from 225 to 186. Increasing the wall thickness will reduce the RF value and accordingly reduce the dye loading on the internal surfaces of the TNT electrodes.

To experimentally confirm the reduced dye loading with the increased TNT wall thickness, absorbance of dyes on the prepared solar cells was measured by desorbing the loaded dyes on the electrodes into 10 mM NaOH. The results are shown in Fig. 6. The spectra show three distinct peaks around 305 nm, 375 nm, and 505 nm, respectively. The two peaks around 375 nm and 505 nm correspond to the metal-to-ligand charge transfer transitions, while the highest energy peak around 305 nm is due to the $\pi \rightarrow \pi^*$ intra ligand transitions [40]. The slight shift of the peak position between different spectra may be attributed to the dye aggregation in a higher concentration solution [40]. As shown in Fig. 6, the absorbance of the desorbed dyes decreases with the increasing $TiO_2$ wall thickness. The experimental tests confirm the decreasing of dye loading and are consistent with the predicted results from the RF calculations. As an example, the inset of Fig. 6 presents the absorbance at 505 nm peak and the calculated roughness factor as a function of the wall thickness. As expected, the reduced RF on $TiO_2$ electrode with increased wall thickness results in relatively low overall light harvesting efficiencies, which consequently reduce the photo-excited electron–hole generation and hence, lead to a

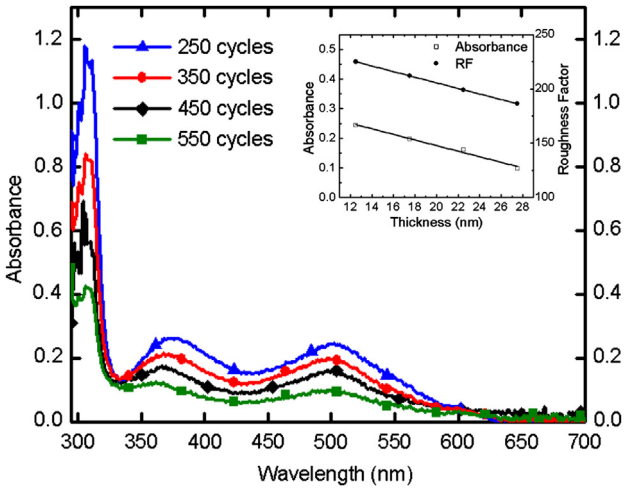


**Fig. 6.** UV–Vis spectra of desorbed N719 dyes from the $TiO_2$ electrodes with different wall thickness. The inset shows absorbance of desorbed dye at around 505 nm and the calculated roughness factor as a function of the $TiO_2$ wall thickness.

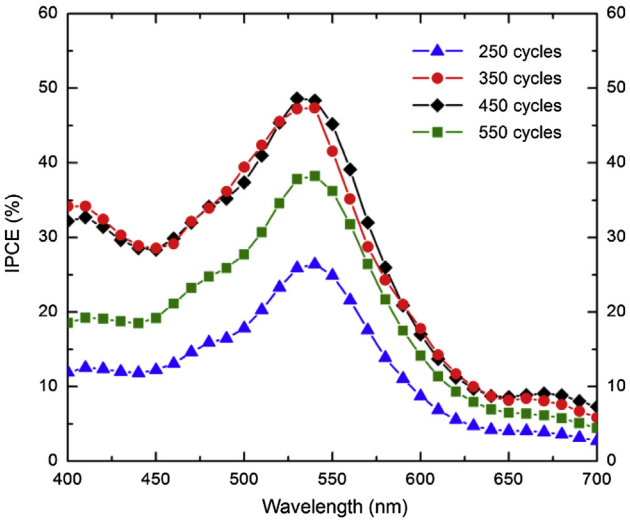


**Fig. 7.** IPCE of fabricated solar cells based on varied wall thickness TNT.

reduced short circuit current density [41]. Overall, it is the competition between the enhanced electron injection/collection and the reduced internal surface area of the electrodes resulting from the increased wall thickness makes 450 cycles sample the best device with the highest photo-conversion efficiency in our tests.

Fig. 7 shows the incident photon-to-current conversion efficiency (IPCE) spectra of the fabricated DSCs based on TNTs with different wall thicknesses. The solar cell with N719 dye shows peak IPCE around 48% at 535 nm, which is in good agreement with the previously published results on dye light absorbance [15]. Analysis of the IPCE spectra for devices constructed with different wall thicknesses reveals that the IPCE values correlate well with the trend of the short circuit current. It is worth noting here that current device performance is optimized only by adjusting the tube wall thickness. However, besides the wall thickness, it is known that nanotube-based photovoltaic performance is also strongly dependent on the length of TNT arrays. With an optimum length of 20 μm, the IPCE of TNT-based solar cells could be improved to 90% [15]. For the free-standing TNT film fabricated by template ALD deposition, other geometry parameters, including the length of tube and the space between tubes, could be controlled precisely. It is anticipated that by further optimizing the nanotube structures the photo-conversion efficiency of DSCs could be further improved.

## 4. Conclusions

In summary, free-standing TNT arrays with ultraprecise controlled wall thickness between 10 and 30 nm range were fabricated by ALD using an AAO template-assisted approach. The obtained TNT films were detached from the substrate without any structural disintegration and then transferred to FTO substrates for fabricating front illuminated DSCs. The study on the dependence of photovoltaic performance on the TNT wall thickness indicates that a thick enough tube wall is crucial for forming space charge layer to allow efficient charge separation, although it will reduce dye loading relatively. An optimal value exists for the best photovoltaic performance. A power conversion efficiency of 4.65% was obtained on the device with 450 ALD cycles of TNT wall thickness in our work. The result provides new insights into design and optimization of photoelectrodes for high-efficiency dye-sensitized solar cells and could be used for enhancing applications of TNT arrays in other nanotechnologies such as photocatalysis and sensors.

## Acknowledgments

The authors thank Dr. Robertson Donald for assistance of TEM characterization, Dr. Heather Oven for discussion about HMDS drying. The financial supports from the Bradley Catalyst Program of the University of Wisconsin, Milwaukee, National Science Foundation (ECCS-1001039) and Department of Energy (DE-EE0003208) are gratefully acknowledged.

## References

[1] B. O'Regan, M. Gratzel, Nature 353 (1991) 737–740.
[2] M. Grätzel, Journal of Photochemistry and Photobiology C: Photochemistry Reviews 4 (2003) 145–153.
[3] M. Grätzel, Inorganic Chemistry 44 (2005) 6841–6851.
[4] M. Law, L.E. Greene, J.C. Johnson, R. Saykally, P. Yang, Nature Materials 4 (2005) 455–459.
[5] Kai Zhu, Nathan R. Neale, Alexander Miedance, A.J. Frank, Nano Letters 7 (2007) 69–74.
[6] N. Wu, J. Wang, D.N. Tafen, H. Wang, J.-G. Zheng, J.P. Lewis, X. Liu, S.S. Leonard, A. Manivannan, Journal of the American Chemical Society 132 (2010) 6679–6685.
[7] S.U.M. Khan, T. Sultana, Solar Energy Materials and Solar Cells 76 (2003) 211–221.
[8] X. Feng, K. Shankar, O.K. Varghese, M. Paulose, T.J. Latempa, C.A. Grimes, Nano Letters 8 (2008) 3781–3786.
[9] K. Shankar, J.I. Basham, N.K. Allam, O.K. Varghese, G.K. Mor, X. Feng, M. Paulose, J.A. Seabold, K.-S. Choi, C.A. Grimes, The Journal of Physical Chemistry C 113 (2009) 6327–6359.
[10] D. Wang, L. Liu, F. Zhang, K. Tao, E. Pippel, K. Domen, Nano Letters 11 (2011) 3649–3655.
[11] X. Xu, X. Fang, T. Zhai, H. Zeng, B. Liu, X. Hu, Y. Bando, D. Golberg, Small 7 (2011) 445–449.
[12] H. Zhang, P. Liu, X. Liu, S. Zhang, X. Yao, T. An, R. Amal, H. Zhao, Langmuir 26 (2010) 11226–11232.
[13] Q. Zheng, H. Kang, J. Yun, J. Lee, J.H. Park, S. Baik, ACS Nano 5 (2011) 5088–5093.
[14] O.K. Varghese, M. Paulose, C.A. Grimes, Nature Nanomaterials 4 (2009) 592–597.
[15] J.R. Jennings, A. Ghicov, L.M. Peter, P. Schmuki, A.B. Walker, Journal of the American Chemical Society 130 (2008) 13364–13372.
[16] L. Sun, S. Zhang, X. Sun, X. He, Journal of Nanoscience and Nanotechnology 10 (2010) 4551–4561.
[17] A. Hagfeldt, M. Graetzel, Chemical Reviews 95 (1995) 49–68.
[18] J.M. Macak, H. Tsuchiya, P. Schmuki, Angewandte Chemie International Edition 44 (2005) 2100–2102.
[19] J.M. Macak, H. Tsuchiya, L. Taveira, S. Aldabergerova, P. Schmuki, Angewandte Chemie International Edition 44 (2005) 7463–7465.
[20] G.K. Mor, O.K. Varghese, M. Paulose, C.A. Grimes, Advanced Functional Materials 15 (2005) 1291–1296.
[21] Z.R. Tian, J.A. Voigt, J. Liu, B. McKenzie, H. Xu, Journal of the American Chemical Society 125 (2003) 12384–12385.
[22] S.-Z. Chu, K. Wada, S. Inoue, S.-i. Todoroki, Chemistry of Materials 14 (2002) 266–272.
[23] M.S. Sander, M.J. Côté, W. Gu, B.M. Kile, C.P. Tripp, Advanced Materials 16 (2004) 2052–2057.
[24] T.R.B. Foong, Y. Shen, X. Hu, A. Sellinger, Advanced Functional Materials 20 (2010) 1390–1396.
[25] L.K. Tan, X. Liu, H. Gao, Journal of Materials Chemistry 21 (2011) 11084.
[26] C. Bae, Y. Yoon, H. Yoo, D. Han, J. Cho, B.H. Lee, M.M. Sung, M. Lee, J. Kim, H. Shin, Chemistry of Materials 21 (2009) 2574–2576.
[27] H. Shin, D.K. Jeong, J. Lee, M.M. Sung, J. Kim, Advanced Materials 16 (2004) 1197–1200.
[28] S.M. George, Chemical Reviews 110 (2009) 111–131.
[29] C.Y. Yuan, D.A. Dornfeld, Journal of Manufacturing Science and Engineering 132 (2010) 030917–030918.
[30] J.A. van Delft, D. Garcia-Alonso, W.M.M. Kessels, Semiconductor Science and Technology 27 (2012) 074002.
[31] J.G. Fan, D. Dyer, G. Zhang, Y.P. Zhao, Nano Letters 4 (2004) 2133–2138.
[32] Y.P. Zhao, J.G. Fan, Applied Physics Letters 88 (2006) 103123.
[33] K. Zhu, T.B. Vinzant, N.R. Neale, A.J. Frank, Nano Letters 7 (2007) 3739–3746.
[34] A.J. Nozik, Annual Review of Physical Chemistry 29 (1978) 189–222.
[35] M. Gratzel, Nature 414 (2001) 338–344.
[36] H. Tang, K. Prasad, R. Sanjinés, P.E. Schmid, F. Leévy, Journal of Applied Physics 75 (1994) 2042.
[37] D. Dung, J. Ramsden, M. Graetzel, Journal of the American Chemical Society 104 (1982) 2977–2985.
[38] J. van de Lagemaat, A.J. Frank, The Journal of Physical Chemistry B 105 (2001) 11194–11205.
[39] J. Ferber, R. Stangl, J. Luther, Solar Energy Materials and Solar Cells 53 (1998) 29–54.
[40] E. Dell'Orto, L. Raimondo, A. Sassella, A. Abbotto, Journal of Materials Chemistry 22 (2012) 11364.
[41] A.B.F. Martinson, J.W. Elam, J.T. Hupp, M.J. Pellin, Nano Letters 7 (2007) 2183–2187.